

Supporting information
for
**Enzyme inhibition-based lab-in-a-syringe device for point-of-
need determination of pesticides**

Limin Yang^{a,*}, Jinxin Wang^a, Linjiao Qu^a, Zhen Liu^{b,c,*}, Lei Jiang^{a,*}

^aState Key Laboratory of Heavy Oil Processing and Center for Bioengineering and Biotechnology, China University of Petroleum (East China), Qingdao 266580, China

^bDepartment of Nuclear Medicine, Union Hospital, Tongji Medical College, Huazhong University of Science and Technology, Wuhan 430022, China

^cHubei Province Key Laboratory of Molecular Imaging, Wuhan 430022, China

*Correspondence: yanglimin@upc.edu.cn (Limin Yang), zhen_liu@hust.edu.cn (Zhen Liu), leijiang@upc.edu.cn (Lei Jiang)

This material includes:

1. Set-up for the EI-LIS device.
2. Peroxidase-like activity of FeTMPyP₄.
3. 1-Naphthol formation in the plant-esterase-catalyzed 1-NA hydrolysis.
4. The inflection point of the kinetic curve.
5. TMB oxidation in the presence of only plant-esterase or 1-NA.
6. Spectral changes of oxTMB after addition of (plant-esterase)+(1-NA).
7. The choice of the pH 3.0 acetate buffered assay solution.
8. Comparison of performance of different detection strategies.
9. Rational design of the two reaction pads.
10. Colorimetric responses to potential inhibitors.
11. Potential interferences in food matrix.
12. Dichlorvos detection in spiked real samples.

References

1. Set-up for the EI-LIS device

As shown in **Fig. S1**, the cartridge is composed of female Luer lock, silicone gasket, and polypropylene support screen with male Luer slip. In the fabrication of conjugate/detection cartridge, the conjugate/detection pad and gasket were sequentially placed on the supported screen, and then the threaded pieces of the cartridge were screwed tightly. Next, conjugate and detection cartridges were serially connected to a standard syringe. The set-up of our EI-LIS device was completed.

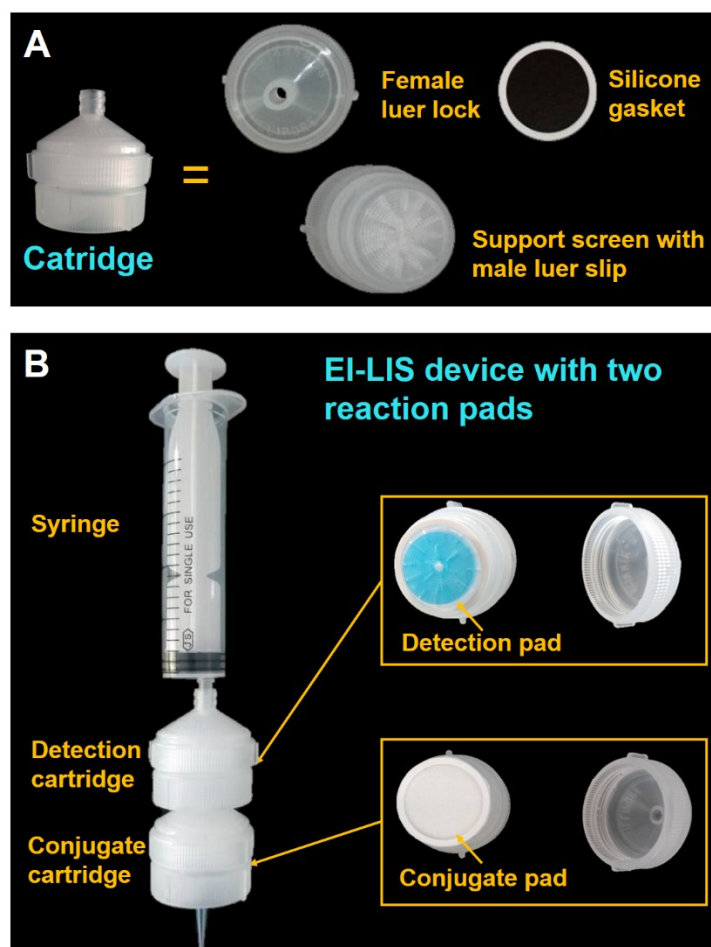


Fig. S1 Photographs of (A) the composition of the cartridge and (B) the set-up used for our EI-LIS device.

2. Peroxidase-like activity of FeTMPyP₄

The peroxidase-like activity of FeTMPyP₄ was characterized in the presence of H₂O₂. As shown in **Fig. S2**, the introduction of FeTMPyP₄ into the solution containing TMB and H₂O₂ results in a typical blue color, whereas no clear color change occurs in the TMB solution in the absence of FeTMPyP₄ or H₂O₂. Therefore, the FeTMPyP₄ possesses intrinsic peroxidase-like activity as reported,¹ and can catalyze the oxidation of the peroxidase substrate TMB in the presence of H₂O₂. The oxidized TMB can produce two intense characteristic absorption peaks at 370 and 658 nm.²

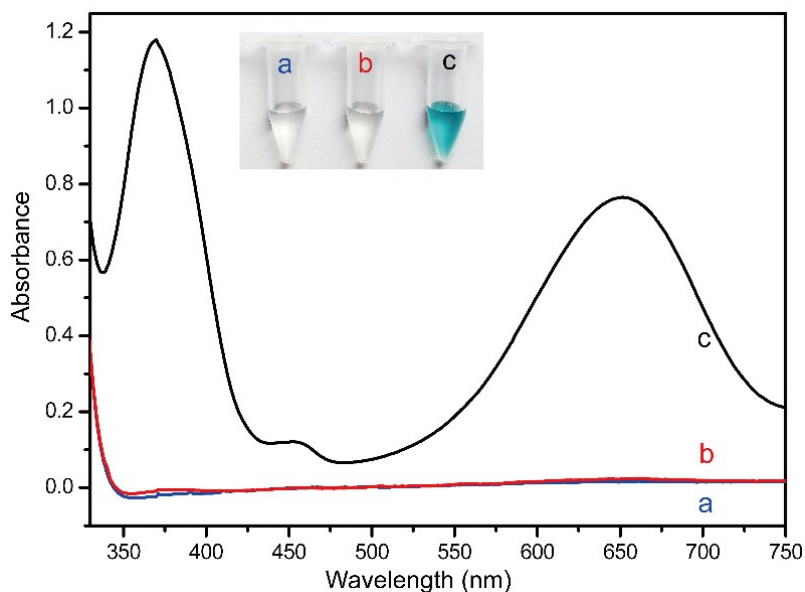


Fig. S2 Typical absorption spectra and images of (a) 1.5 mM TMB, (b) 1.5 mM TMB + 2 mM H₂O₂, and (c) 1 μM FeTMPyP₄ + 1.5 mM TMB + 2 mM H₂O₂ in 0.2 M acetate buffer, pH 3.0.

3. 1-Naphthol formation in the plant-esterase-catalyzed 1-NA hydrolysis

Acetate buffer (0.2 M, pH 3.0) was used as the supporting solution. The reaction of 1-NA was started by adding plant-esterase to the substrate media, and then immediately spectrophotometrically monitored by the spectrophotometer at 25 °C.

Fig. S3 shows time-dependent spectra scan of the enzyme reaction and the corresponding absorbance intensity-reaction time curves. Upon the initiation of the reaction, the absorption peak was centered at 268 nm, and no absorption peak centered at 321 nm, typical of 1-naphthol absorbance,³ was observable. As the reaction went on, the peak at 268 nm decreased while the peak at 321 nm increased gradually, with a clear isosbestic point at 290 nm, suggesting the conversion of 1-NA to 1-naphthol; the process completed in ~120 min.

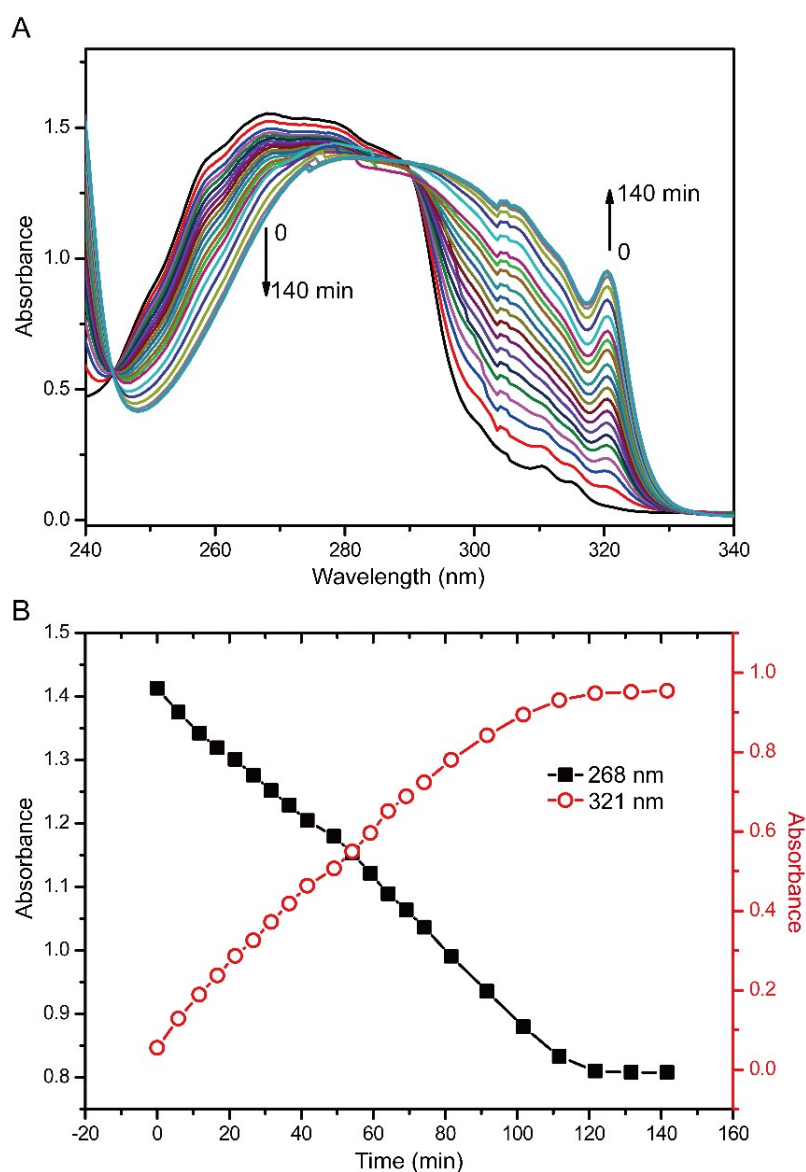


Fig. S3 Time-dependent spectral changes in the plant-esterase-catalyzed hydrolysis of 1-NA in 0.2 M acetate buffer, pH 3.0. [Plant-esterase] = 36 mU mL⁻¹, [1-NA] = 0.5 mM.

4. The inflection point of the kinetic curve

The point of inflection in the induction period was determined by plotting the second derivative of the TMB oxidation curve with respect to time (Fig. S4). The point of inflection is where the second derivative is zero⁴.

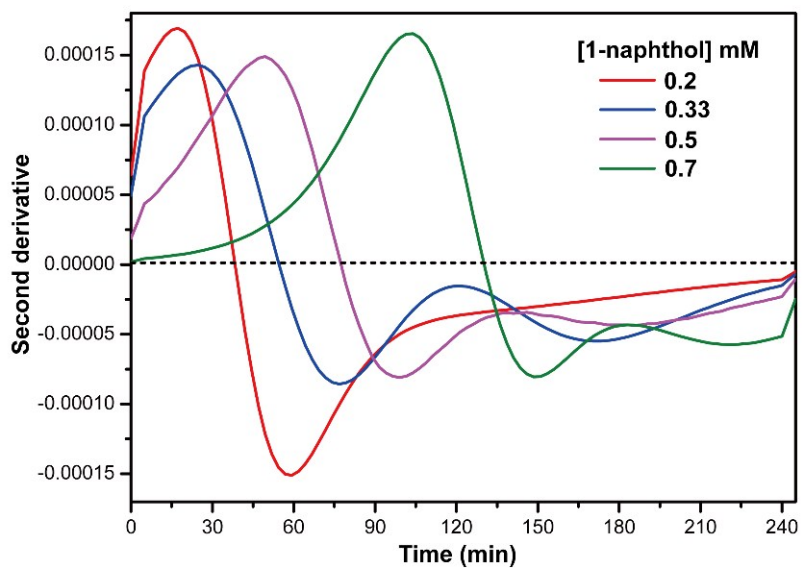


Fig. S4 The second derivative of the TMB oxidation curves with respect to time.

5. TMB oxidation in the presence of only plant-esterase or 1-NA

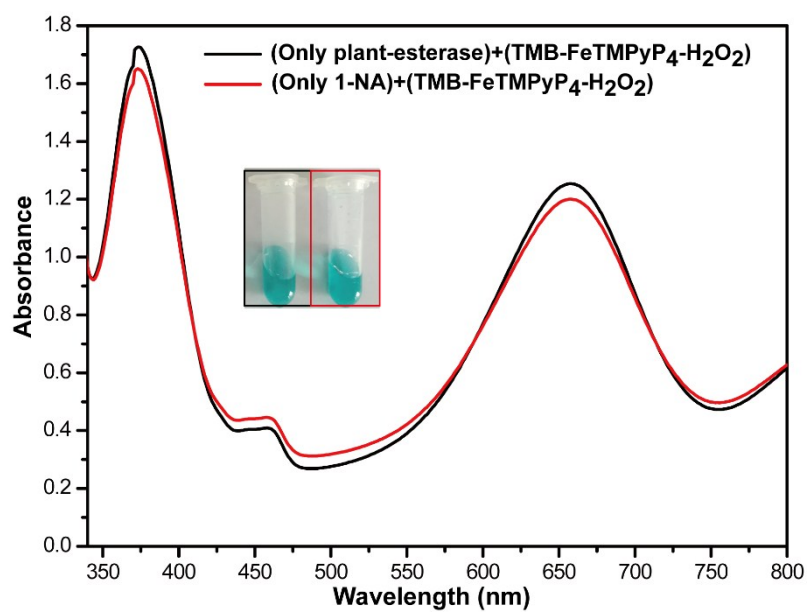


Fig. S5 FeTMPyP₄-catalyzed oxidation of TMB in the absence of either plant-esterase (black curve) or 1-NA (red curve). Inset: the corresponding photographs of reaction solutions.

6. Spectral changes of oxTMB after addition of (plant-esterase)+(1-NA)

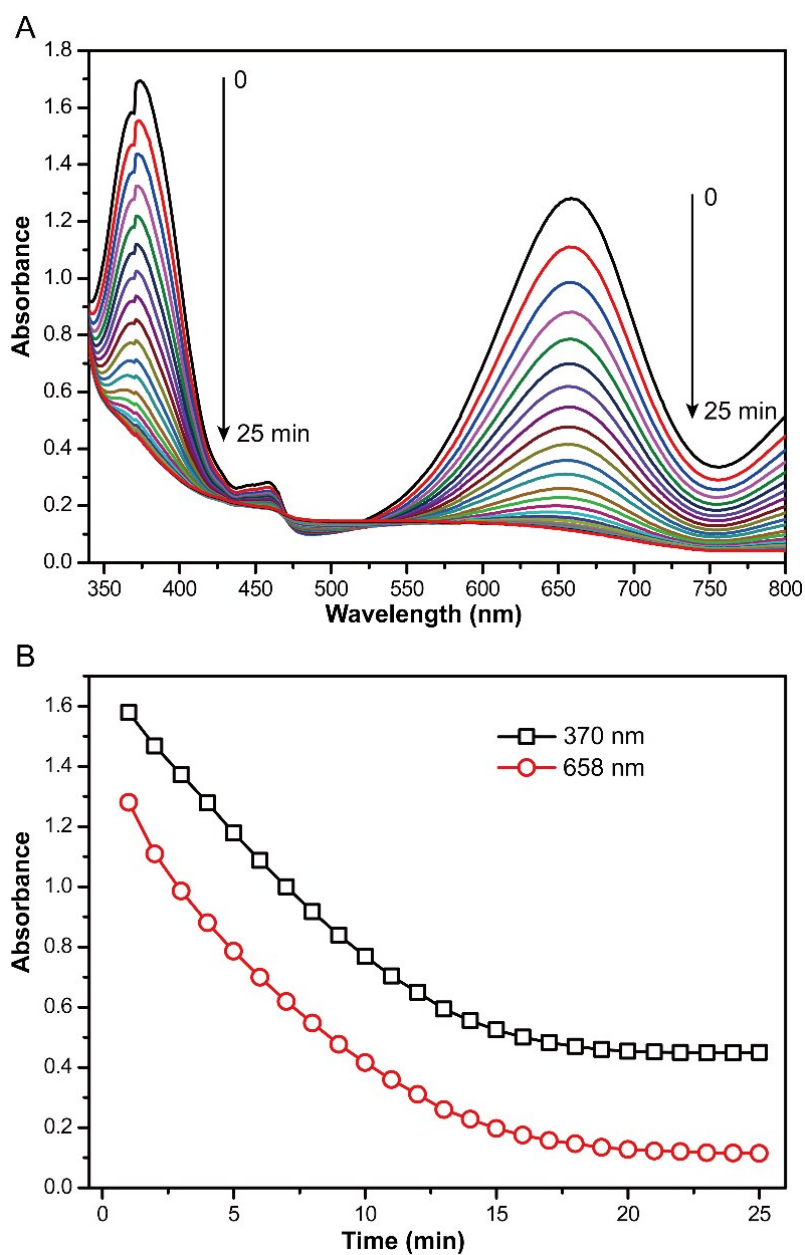


Fig. S6 (A) Time-dependent changes in the spectra of oxTMB after addition of (plant-esterase)+(1-NA) and (B) the corresponding absorbance intensity-reaction time curves.

7. The choice of the pH 3.0 acetate buffered assay solution

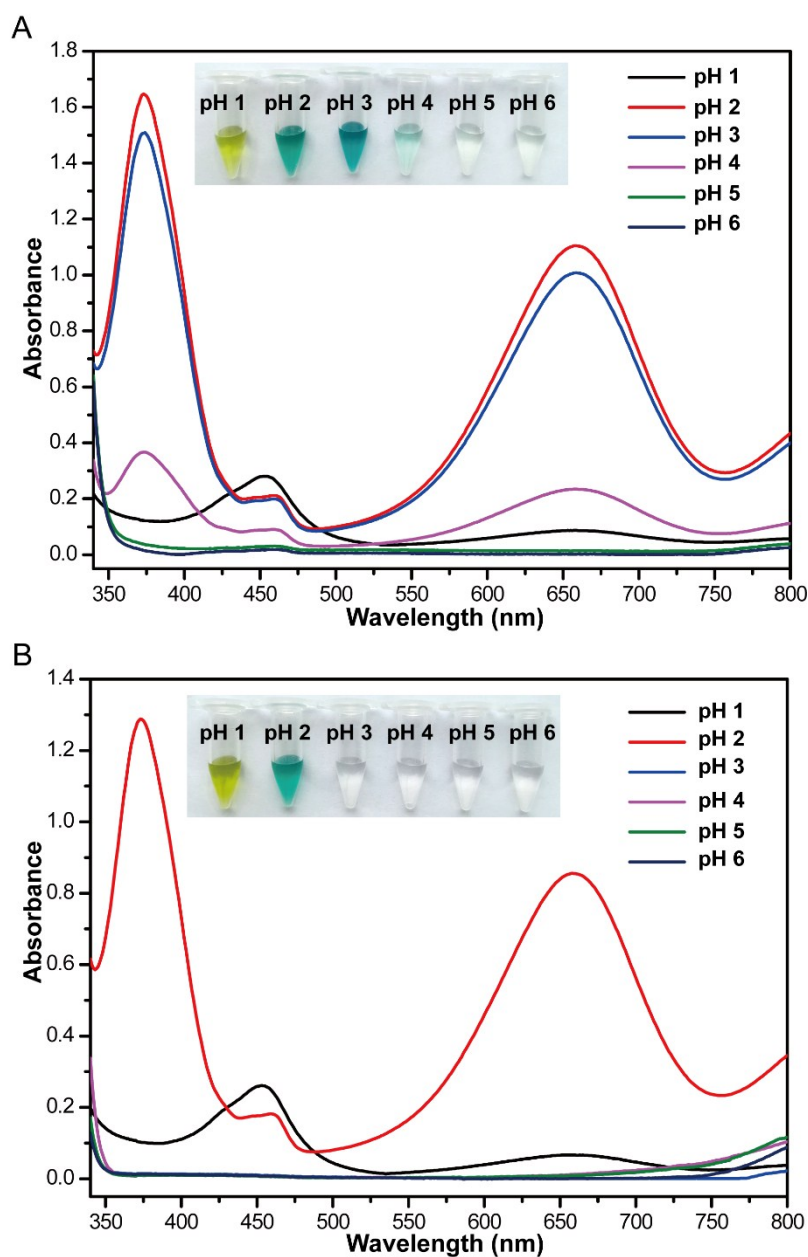


Fig. S7 FeTMPyP₄-catalyzed oxidation of TMB at different pHs in the absence (A) and presence of (plant-esterase)+(1-NA) (B). The assay media was either concentrated HCl (pH 1.0, and 2.0) or acetate buffer (0.2 M, pH 3.0-6.0). The pH values were checked precisely by a FE-20 pH-meter (Mettler Toledo, China).

8. Comparison of performance of different detection strategies

Table S1 Comparison of performance of different dichlorvos detection strategies based on AChE inhibition

Methods	Linear range (nM)	Detection limit (nM)	Reference
Electrochemical detection using a Pt electrode modified with ZnO nano-interface and AChE matrix	Not mentioned	0.012	5
An electrochemical AChE biosensor based on doping Au nanorod@SiO ₂ nanoparticles into TiO ₂ -chitosan hydrogel	18 ~ 13600	5.3	6
A fluorescence resonance energy transfer biosensor based on carbon dots and the traditionally colorimetric Ellman's test	0.05 ~ 100	0.019	7
A fluorescent sensor coupling the carbon-dots-Cu(II) system with AChE-acetylthiocholine system	6.0 ~ 60	3.8	8
Colorimetric assay coupling the peroxidase-mimicking properties of platinum nanoparticles with AChE-acetylthiocholine system	Not mentioned	10	9
Visual detection using QD-AChE aerogel based microfluidic arrays	0.001 ~ 10000	0.012	10
A colorimetric paper sensor based on the domino reaction of acetylcholinesterase and degradable γ -MnOOH nanozyme	4.5 ~ 45	13.5	11
Colorimetric assay based on a 1-naphthol-linked bi-enzymatic reaction	0.01 ~ 1000	0.00036	This work
Colorimetric assay using our EI-LIS device	0.1 ~ 10000	0.07	This work

9. Rational design of the two reaction pads

The installation of the bi-enzymatic reaction into the LIS device relies on the rational design of two reaction pads.

One pad immobilized with plant-esterase is used as the conjugate pad, which not only captures the inhibitor, but also mediates the hydrolysis of 1-NA to generate 1-naphthol. Among the available methods for enzyme immobilization, four methods are currently used: physical adsorption, entrapment in a gel or polymer, cross-linking, and covalent coupling to support.¹² The entrapment of a layer of cross-linked enzymes with glutaraldehyde into robust membranes has been used to reduce the leakage of enzymes and to improve the analytical performances due to a reduction of the interference and a diffusion limit of the substrate. Several membranes, including cellulose acetate, glass fiber, polyester fiber, and filter paper, were tried. Polyester fiber membrane was finally selected to immobilize the plant-esterase due to its excellent tenacity and water-absorbing quality. BSA was also introduced in the immobilization to provide the enzyme a proteic environment that is favorable for its stability.¹³

The other pad immobilized with the oxTMB from FeTMPyP₄-catalyzed TMB oxidation is the detection pad for signaling the captured inhibitor. It is necessary to ensure that the enzymatic product 1-naphthol can pass through the pad matrix to react with the oxTMB, and also, the color changes of oxTMB can be observed directly by the naked eyes. Agarose seems to be an ideal substrate for chromogenic reaction for the following three reasons: (i) the network structure of agarose gel allows small molecules to pass through; (ii) the transparency is not only convenient to qualitative observation of color changes, but also enables quantitative measurement possible with the assist of conventional UV-vis absorption spectrometer; (iii) it is easy to process through simple heating and cooling treatment. Therefore, agarose gel was selected to entrap the oxTMB. To reduce the pressure during the reciprocating pumping of the syringe, the size of the detection pad is smaller than the inner diameter of the cartridge, and a hole is left in the center of the pad. These two pads were finally inserted inside two plastic cartridges and connected to the syringe, and the EI-LIS device was fabricated (**Fig. S1**).

10. Colorimetric responses to potential inhibitors

According to the working principle, our EI-LIS device is expected to be effective for other toxins, which can inhibit plant-esterase activity. To verify this, colorimetric responses of this device to several potential inhibitors were also investigated, including organophosphorus pesticides (omethoate, chlorpyrifos, malathion), carbamate pesticides (ziram, thiram, thiodicarb), Cd^{2+} (heavy metal), mycotoxins (aflatoxin, ochratoxin), acetamiprid (neonicotinoid insecticide), and atrazine (triazine herbicide). As shown in **Fig. S8**, the appearance of blue color is observed on the detection pad for organophosphorus and carbamate pesticides, and Cd^{2+} , while the blank sample and other toxins give colorless detection pads. To make a further confirmation, absorbance at 609 nm was also measured. All the blue detection pads have strong absorption at 609 nm.

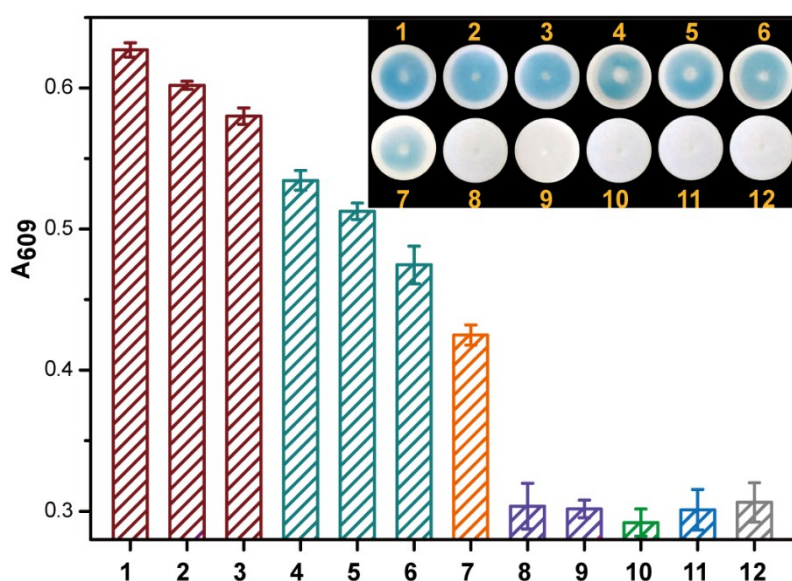


Fig. S8 Response to other toxins: 1, dichlorvos, 2, omethoate, 3, chlorpyrifos, 4, ziram, 5, thiram, 6, thiodicarb, 7, Cd^{2+} , 8, aflatoxin B1, 9, ochratoxin A, 10, acetamiprid, 11, atrazine, 12, blank. The concentrations of all the toxins are 1 μM .

11. Potential interferences in food matrix

The signal responses of the EI-LIS assay toward the potential interfering substances coexisting in food were studied. As shown in **Fig. S9**, no obvious interferences are noticed with the presence of interfering species including metal ions (Fe^{2+} , K^+ , and Na^+) and saccharides (glucose and sucrose). Whereas, the interferences from antioxidants (vitamin C, vitamin E, catechol, and quercetin) cannot be ignored. It is well accepted that β -carotene could alleviate the oxidation of TMB. However, the co-existing β -carotene does not disturb the EI-LIS assay. The probable reason is that the poor water solubility of β -carotene affects its entry into the agarose network to reduce the oxTMB. A similar situation occurs in the assay co-existing vitamin E.

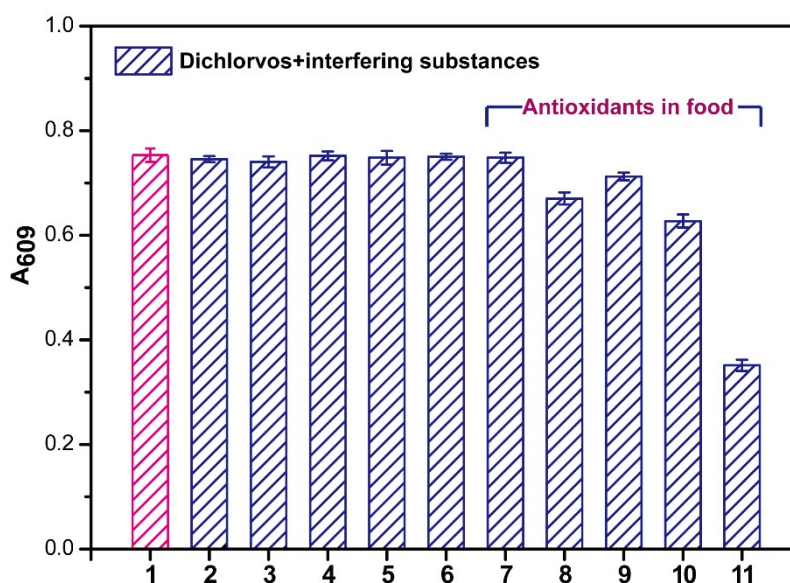


Fig. S9 Effect of co-existing substances on the dichlorvos ($10 \mu\text{M}$) assay: 1, control; 2, Fe^{2+} ; 3, K^+ ; 4, Na^+ ; 5, glucose; 6, sucrose; 7, β -carotene; 8, vitamin C; 9, vitamin E; 10, catechol; 11, quercetin. All the concentrations of these interfering substances are $10 \mu\text{M}$.

12. Dichlorvos detection in spiked real samples

Table S2 Results of the determination of dichlorvos in spiked real samples

Samples	Spiked (nM)	Found (nM)	Recovery (%)	RSD (%)
Chinese cabbage	1	0.95	95.12	3.73
	10	9.42	94.20	2.21
	100	97.64	97.64	2.99
Cabbage	1	0.94	93.79	3.26
	10	9.51	95.06	4.22
	100	96.69	96.69	3.16
Lettuce	1	0.94	93.93	4.92
	10	9.45	94.47	2.45
	100	96.26	96.26	3.17

References

- 1 Y. Zhou, X. Huang, W. Zhang, Y. Ji, R. Chen and Y. Xiong, *Biosens. Bioelectron.*, 2018, **102**, 9-16.
- 2 P. D. Josephy, T. Eling and R. P. Mason, *J. Biol. Chem.*, 1982, **257**, 3669-3675.
- 3 V. D. Trivedi, P. K. Jangir, R. Sharma and P. S. Phale, *Sci. Rep.*, 2016, **6**, 38430.
- 4 L. I. Sly, L. L. Blackall, P. C. Kraat, T. Tian-Shen and V. Sangkhobol, *J. Microbiol. Methods*, 1986, **5**, 139-156.
- 5 R. Sundarmurugasan, M. B. Gumpu, B. L. Ramachandra, N. Nesakumar, S. Sethuraman, U. M. Krishnan and J. B. B. Rayappan, *Sens. Actuators B*, 2016, **230**, 306-313.
- 6 H.-F. Cui, T.-T. Zhang, Q.-Y. Lv, X. Song, X.-J. Zhai and G.-G. Wang, *Biosens. Bioelectron.*, 2019, **141**, 111452.
- 7 J. Hou, Z. Tian, H. Xie, Q. Tian and S. Ai, *Sens. Actuators B*, 2016, **232**, 477-483.
- 8 J. Hou, G. Dong, Z. Tian, J. Lu, Q. Wang, S. Ai and M. Wang, *Food Chem.*, 2016, **202**, 81-87.
- 9 J. Cao, M. Wang, Y. She, A. M. Abd El-Aty, A. Hacimüftüoğlu, J. Wang, M. Yan, S. Hong, S. Lao and Y. Wang, *Microchim. Acta*, 2019, **186**, 390.
- 10 T. Hu, J. Xu, Y. Ye, Y. Han, X. Li, Z. Wang, D. Sun, Y. Zhou and Z. Ni, *Biosens. Bioelectron.*, 2019, **136**, 112-117.
- 11 L. Huang, D.-W. Sun, H. Pu, Q. Wei, L. Luo and J. Wang, *Sens. Actuators B*, 2019, **290**, 573-580.
- 12 M. A. T. Gilmartin, J. P. Hart and D. T. Patton, *Analyst*, 1995, **120**, 1973-1981.
- 13 R. Sternberg, D. S. Bindra, G. S. Wilson and D. R. Thevenot, *Anal. Chem.*, 1988, **60**, 2781-2786.